Supplement

Contents: Sect. S1 (rate calculations), Figs. S1–S8, Tables S1–S6.

S1 Rate calculations

All rates were calculated per core from the measured height of the overlying water (h_w). Because the volume of overlying water is $V_w = A\,h_w$, where A is the internal cross-sectional area of the core tube, the conversion of a volumetric rate in the overlying water to an areal rate, V_w / A, equals h_w (10 L m^{-2} per cm of water) and does not depend on A; in Eqs. (S3), (S6a), and (S7) h_w is therefore expressed in L m^{-2}. The porewater volume was not included. Slopes (S) were obtained by linear regression of the dilution-corrected quantity against time over the sampling points (0–72 h, every 12 h). All rates are expressed in µmol N m^{-2} h^{-1} (µmol N_2 m^{-2} h^{-1} multiplied by 2 for N_2 fluxes). The calculations for every core, with all formulas, are provided in the data repository (files denitrification_calculation.xlsx, N2flux_calculation.xlsx and DNRA_calculation.xlsx), and the time series of every core are shown in Figs. S6–S8.

S1.1 Dilution correction

At each sampling time the volume of overlying water withdrawn (V_s) was replaced with site water, which contained dissolved N_2 at air equilibrium and at natural isotopic abundance; $f_j = V_{s,j} / V_w$ is the fraction of the overlying water replaced after sampling j. For the N_2 series of the ^{15}N-amended cores, the replacement water dilutes only the ^{15}N-labelled N_2 that has accumulated, not the natural-abundance background. The correction was therefore applied to the excess of each isotope ratio over its natural-abundance value measured on our instrument, $E = R - R_{nat}$ (R_{nat} = 0.00731 for $^{29}N_2$:$^{28}N_2$ and 0.00015 for $^{30}N_2$:$^{28}N_2$; the value for $^{30}N_2$:$^{28}N_2$ exceeds the theoretical natural-abundance ratio of 1.3×10^{-5} because it includes the instrument background at *m/z* 30, and using the theoretical value instead changes the denitrification rates by < 1 % on average and by at most 1.3 % in individual cores), for the water replaced after the previous sampling, in the same way as for the control cores (Eq. (S1b)):

$$E_{corr}(t_k) = E(t_k) / (1 - f_{k-1}). \quad \text{(S1a)}$$

For the unamended control cores, the N_2 concentration (C, µmol L^{-1}; from the N_2:Ar ratio and the air-equilibrium Ar concentration at the incubation temperature; Kana et al., 1994) was corrected

by mass balance for the air-equilibrated replacement water (concentration C_{eq}) added after the previous sampling:

$$C_{corr}(t_k) = [C(t_k)\, V_w - C_{eq}\, V_{s,k-1}] / (V_w - V_{s,k-1}). \quad \text{(S1b)}$$

S1.2 Potential denitrification (cores amended with 50 µmol L^{-1} $Na^{15}NO_3$)

Let S_{29} and S_{30} be the slopes (h^{-1}) of the corrected excess $^{29}N_2$:$^{28}N_2$ and $^{30}N_2$:$^{28}N_2$ ratios (Eq. (S1a)) against time. Production rates in the overlying water (µmol N_2 L^{-1} h^{-1}) are

$$P_{29} = S_{29} \times [N_2]_{eq}, \quad P_{30} = S_{30} \times [N_2]_{eq}, \quad \text{(S2)}$$

where $[N_2]_{eq}$ (µmol L^{-1}) is the air-equilibrium N_2 concentration at the incubation temperature, taken as the $^{28}N_2$ concentration (577.7 µmol L^{-1} at the incubation temperature of 16 °C; Hamme and Emerson, 2004). Areal production rates (µmol N_2 m^{-2} h^{-1}) are

$$p_{29} = P_{29}\, h_w, \quad p_{30} = P_{30}\, h_w. \quad \text{(S3)}$$

Following the isotope pairing technique (Nielsen, 1992), denitrification of the ^{15}N-labelled and unlabelled NO_3^- pools (µmol N m^{-2} h^{-1}) and the total potential denitrification rate are

$$D_{15} = p_{29} + 2\, p_{30}, \quad D_{14} = D_{15} \times p_{29} / (2\, p_{30}), \quad D_{tot} = D_{14} + D_{15}. \quad \text{(S4)}$$

The ^{15}N atom fraction of the NO_3^- pool undergoing reduction in each core follows from the same pairing:

$$F_{NO3} = 2\, p_{30} / (p_{29} + 2\, p_{30}) = D_{15} / D_{tot}. \quad \text{(S5)}$$

The IPT assumes random pairing within a single NO_3^- pool and negligible anammox (Risgaard-Petersen et al., 2003); anammox was not detected (Sect. S1.4), so the latter assumption was met. The dilution-corrected ratios of every core are shown in Fig. S6.

S1.3 Potential DNRA (same cores as S1.2; $^{15}NH_4^+$ by OX/MIMS)

Samples for $^{15}NH_4^+$ were frozen (−20 °C, without acidification) and stored for 12–20 months until they were analysed in three batches, in October and November 2024. They were thawed, transferred without bubbles to 6 mL Exetainers and purged by bubbling with high-purity N_2 at the incubation temperature to remove the dissolved gases (including $^{29}N_2$ and $^{30}N_2$ produced by denitrification during the incubation) and to replace them with N_2 at natural isotopic abundance. Alkaline hypobromite iodine solution (0.1 mL) was then injected to oxidize NH_4^+ to N_2 (Yin et

al., 2014). The oxidant was prepared by adding 10 mL of bromine dropwise to 60 mL of 16 mol L^{-1} low-N NaOH at < 5 °C with continuous stirring, storing the solution refrigerated for one week, removing the NaBr precipitate by filtration and mixing the supernatant with an equal volume of 0.2 % (w/v) KI solution. The concentrations of $^{29}N_2$ and $^{30}N_2$ in each vial (µmol L^{-1}) were calculated as $[^{29}N_2] = R_{29}\,[N_2]$ and $[^{30}N_2] = R_{30}\,[N_2]$, where R_{29} and R_{30} are the drift-corrected $^{29}N_2$:$^{28}N_2$ and $^{30}N_2$:$^{28}N_2$ ratios and $[N_2]$ is the N_2 concentration of the vial derived from the mass-28 signal with a two-point calibration against air-equilibrated water at 10 and 20 °C in each batch (Kana et al., 1994); in the purged vials $[N_2]$ was mostly 700–850 µmol L^{-1}. The mass-30 signal was corrected for the instrument background by subtracting the lowest mass-30 reading of the 20 °C air-equilibrated standards of the same standardization interval before the ratio was formed. The ^{15}N in the gas, $[^{15}N]_{gas} = [^{29}N_2] + 2\,[^{30}N_2]$, was converted to the $^{15}NH_4^+$ concentration (µmol N L^{-1}) with the linear calibration $[^{15}N]_{gas} = m\,[^{15}NH_4^+] + b$ fitted to NH_4Cl standards (400 µmol N L^{-1}; 0 %, 5 %, 10 %, 15 %, and 20 % ^{15}N, i.e. 0–80 µmol $^{15}NH_4^+$ L^{-1}; three replicates each, two at 20 %) that were purged, oxidized, and analysed in the same way as the samples, in August 2024, and processed with the same drift and background corrections (m = 0.79, b = 8.5 µmol L^{-1}, r^2 = 0.99); check standards of the same series were analysed in each sample batch to verify the calibration. No natural-abundance value was subtracted, the ^{15}N carried by the N_2 of the purged vials being accounted for by the intercept (Yin et al., 2014). The unlabelled standards had a $^{29}N_2$:$^{28}N_2$ ratio of 0.00713 ± 0.00007, i.e. natural abundance at the instrument settings of these batches (cf. 0.00731 for the incubation samples, Sect. S1.1). The method detection limit, defined as three standard deviations of $[^{15}N]_{gas}$ of the unlabelled standards divided by m, was 0.6 µmol $^{15}NH_4^+$ L^{-1}. Because the standards held more N_2 (830–950 µmol L^{-1}) than most incubation vials, the $^{15}NH_4^+$ concentrations from the calibration carry an offset in each vial (the ^{15}N of the natural-abundance N_2 of the purged vial, which scales with its N_2 content); the time series were therefore expressed as the $^{15}NH_4^+$ produced since the start of the incubation, $[^{15}NH_4^+](t) - [^{15}NH_4^+](0)$, which removes the offset of the 0 h vial, and corrected at each sampling for the water replaced after the previous sampling (Eq. (S1a) applied to this quantity). Let S_{15NH4} (µmol N L^{-1} h^{-1}) be the slope of the $^{15}NH_4^+$ produced against time. The areal production of $^{15}NH_4^+$ (Gardner et al., 2006; McCarthy et al., 2016) is

$$\mathrm{DNRA}_{15} = S_{15NH4}\,h_w \quad (\mu\mathrm{mol\ N\ m^{-2}\ h^{-1}}), \quad \text{(S6a)}$$

which refers to the ^{15}N-labelled NO_3^- pool. The potential DNRA rate reported in the main text is scaled to the whole NO_3^- pool by dividing by the ^{15}N atom fraction of the overlying-water NO_3^- pool after tracer addition, $F_{ow} = 50 / (50 + [NO_3^-]_0)$, where $[NO_3^-]_0$ (µmol L^{-1}) is the ambient NO_3^- concentration of the core before tracer addition (Risgaard-Petersen and Rysgaard, 1995; Dong et al., 2009):

$$\mathrm{DNRA} = \mathrm{DNRA}_{15} / F_{ow}\ (\mu\mathrm{mol\ N\ m^{-2}\ h^{-1}}). \quad \text{(S6b)}$$

F_{ow} was 0.29–0.61 in the June–October cores (0.34–0.49 in March). In one October core without mats (and in one March core without mats) the $^{15}NH_4^+$ slope was slightly negative (−0.1 and −0.03 µmol N m^{-2} h^{-1} before scaling) and the DNRA rate was set to zero. The time series of every core are shown in Fig. S8.

Because anammox was not detected, no correction for anammox consumption of $^{15}NH_4^+$ (Song et al., 2016) was required. The DNRA rates are potential because the added tracer increased the overlying-water NO_3^- concentration by about 50–115 % (monthly means). The share of DNRA in NO_3^- reduction was calculated as DNRA / (DNRA + D_{tot}).

S1.4 Possible anammox (cores amended with 50 µmol L^{-1} $^{15}NH_4Cl$)

With S_{29} the slope of the corrected $^{29}N_2$:$^{28}N_2$ ratio in the $^{15}NH_4^+$-amended cores, p_{29} was calculated as in Eqs. (S2)–(S3). Anammox combines one N atom from NH_4^+ with one from NO_2^-, so the possible anammox rate (µmol N m^{-2} h^{-1}) is 2 p_{29} / F_{NH4}, where F_{NH4} is the ^{15}N atom fraction of the overlying-water NH_4^+ pool after tracer addition (Song et al., 2016). Because $^{29}N_2$ may also arise from nitrification of the added $^{15}NH_4^+$ followed by denitrification, this quantity includes any such coupled nitrification–denitrification as well as anammox. In all cores, S_{29} did not differ from zero, so no anammox rate was computed. The method detection limit was calculated from the replicate unlabelled standards of the $^{15}NH_4^+$ calibration (Sect. S1.3), whose $^{29}N_2$:$^{28}N_2$ ratio had a standard deviation of 7.3×10^{-5} (n = 3). A change in $^{29}N_2$:$^{28}N_2$ of three standard deviations (2.2×10^{-4}) over the 72 h incubation corresponds to p_{29} = 0.26 µmol N_2 m^{-2} h^{-1} for a core with 15 cm of overlying water (Eqs. (S2)–(S3)), i.e. to a possible anammox rate of approximately 1.1 µmol N m^{-2} h^{-1} with F_{NH4} = 0.5 (0.43–0.99 in the cores; 0.6–1.8 µmol N m^{-2} h^{-1} over the 8–26 cm range of water heights of the $^{15}NO_3^-$-amended cores; the water heights of the $^{15}NH_4^+$-amended cores were not recorded).

S1.5 Net sediment–water N_2 flux (control cores without tracer)

With S_{28} (μmol N_2 L^{-1} h^{-1}) the slope of the dilution-corrected N_2 concentration (Eq. (S1b)) against time, the net areal N_2 flux is

$$J_{N2} = 2\, S_{28}\, h_w \quad (\mu\text{mol N m}^{-2}\ \text{h}^{-1}). \quad \text{(S7)}$$

Positive values (a net flux from the sediment to the water column) indicate net N_2 production (denitrification plus anammox exceeding N_2 fixation); negative values (a net flux from the water column into the sediment) indicate net N_2 consumption (N_2 fixation exceeding denitrification). The N_2:Ar ratios and the dilution-corrected N_2 concentrations of every core are shown in Fig. S7.

Supplementary figures

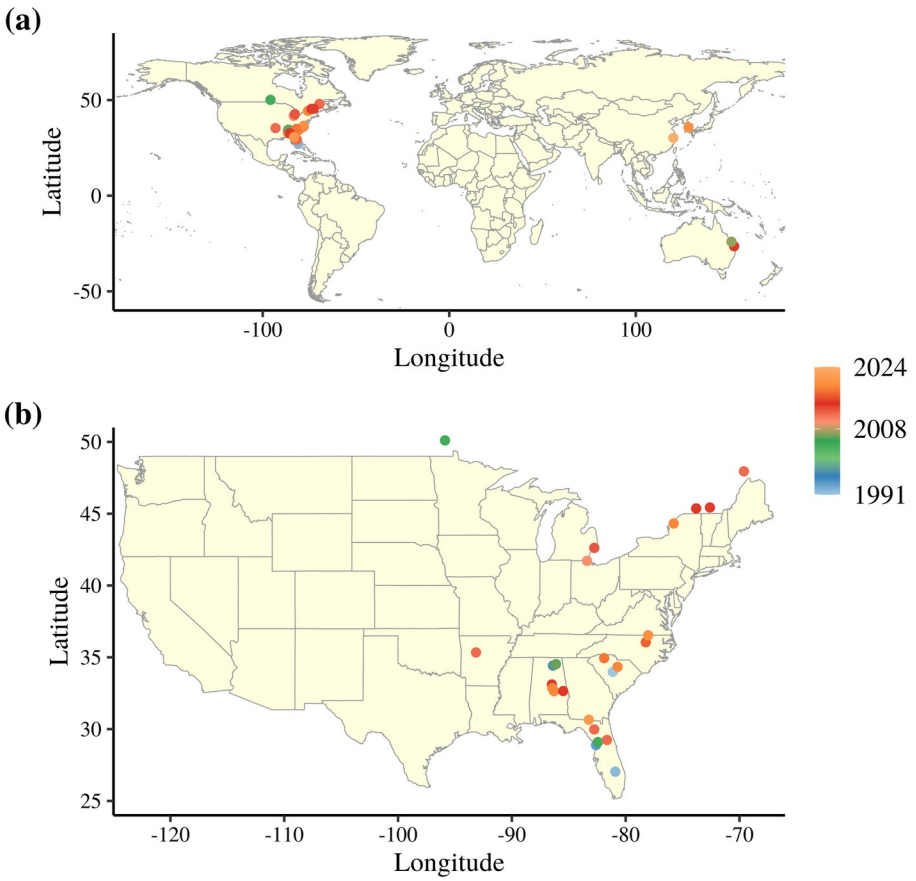


Figure S1. (a) Global and (b) United States distribution of *M. wollei* records in the scientific literature from 1991 to 2024. Colours indicate the year of the record.

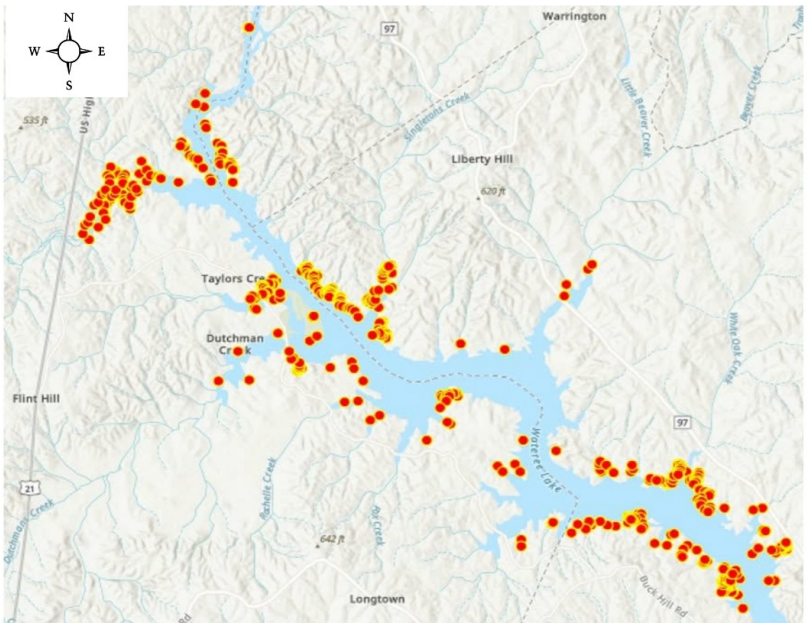


Figure S2. Survey of *M. wollei* benthic mats conducted by the Lake Wateree Association on Lake Wateree, South Carolina, in spring 2025. The survey postdates the sampling reported here, and mat cover varies between years. Red circles indicate the presence of benthic mats. The fraction of the shoreline affected by mats quoted in Sect. 2.1 of the main text (roughly a third to a half) was estimated from this map by image analysis (R script in the data repository): the lake was identified by its colour, its outline was divided into square cells, and the percentage of cells containing a survey marker was counted; it is 34 % for cells of 20 pixels and 49 % for cells of 30 pixels (two to three marker diameters).

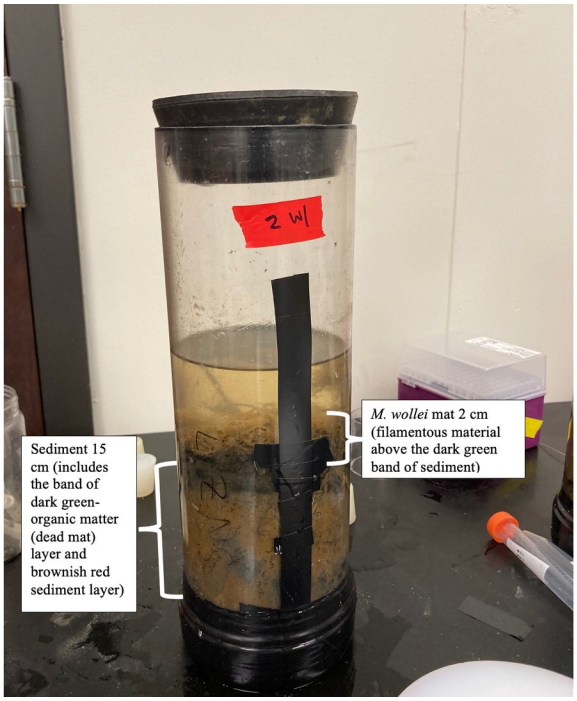


Figure S3. Example core showing how the *M. wollei* mat (filamentous material above the dark green band) was distinguished from the underlying sediment (dark green organic-rich layer of dead mat material overlying brownish-red sediment) when measuring mat thickness.

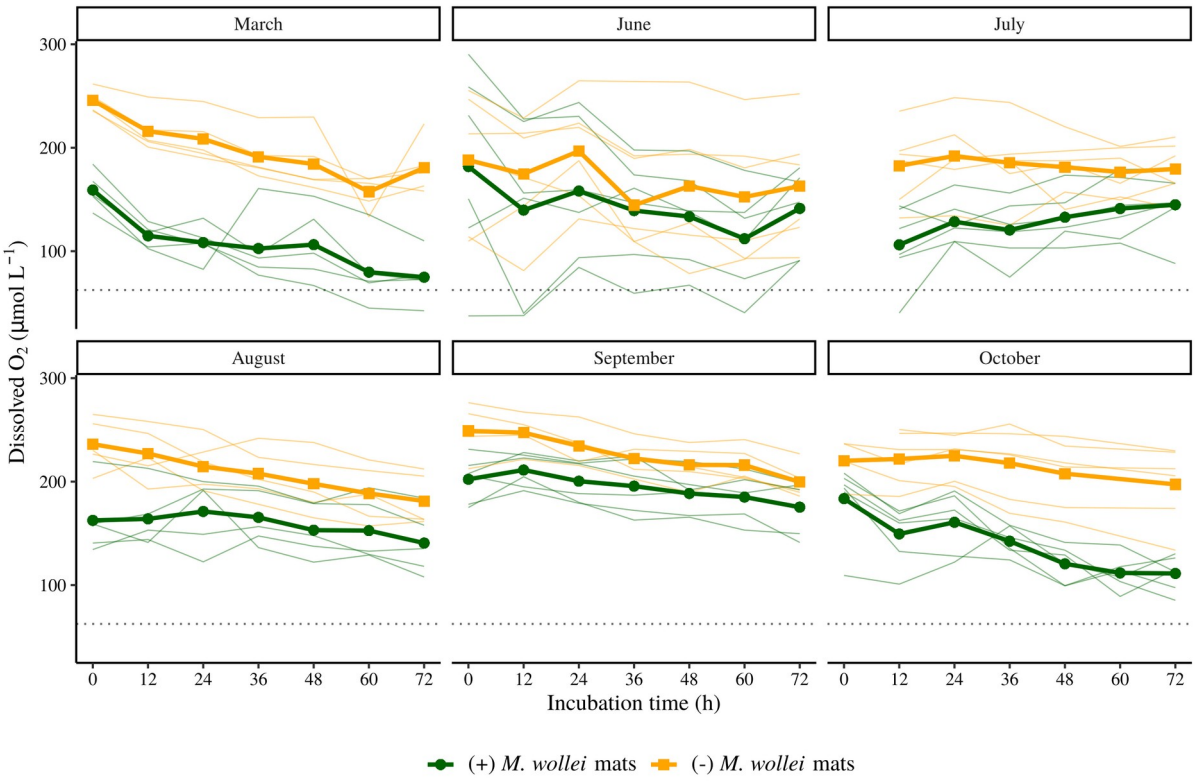


Figure S4. Dissolved O_2 in the overlying water of all incubated cores ($^{15}NO_3^-$-amended, $^{15}NH_4^+$-amended, and unamended control cores) over the 72 h incubations, by month. Bold lines are means and thin lines are individual cores; green circles are cores with *M. wollei* mats and orange squares are cores without mats. The dotted horizontal line marks 62.5 µmol O_2 L^{-1} (2 mg L^{-1}). In July the first reading was taken at 12 h. Summary statistics are given in Table S2.



Figure S5. Porewater nutrient profiles (NH_4^+, NO_2^-, NO_3^-, PO_4^{3-}, and total Fe; mg N, P, or Fe L^{-1}) in cores with (green) and without (orange) *M. wollei* mats, shown separately for the light (transparent symbols) and dark (solid symbols) treatments. Statistical tests of the light effect are given in Table S3.

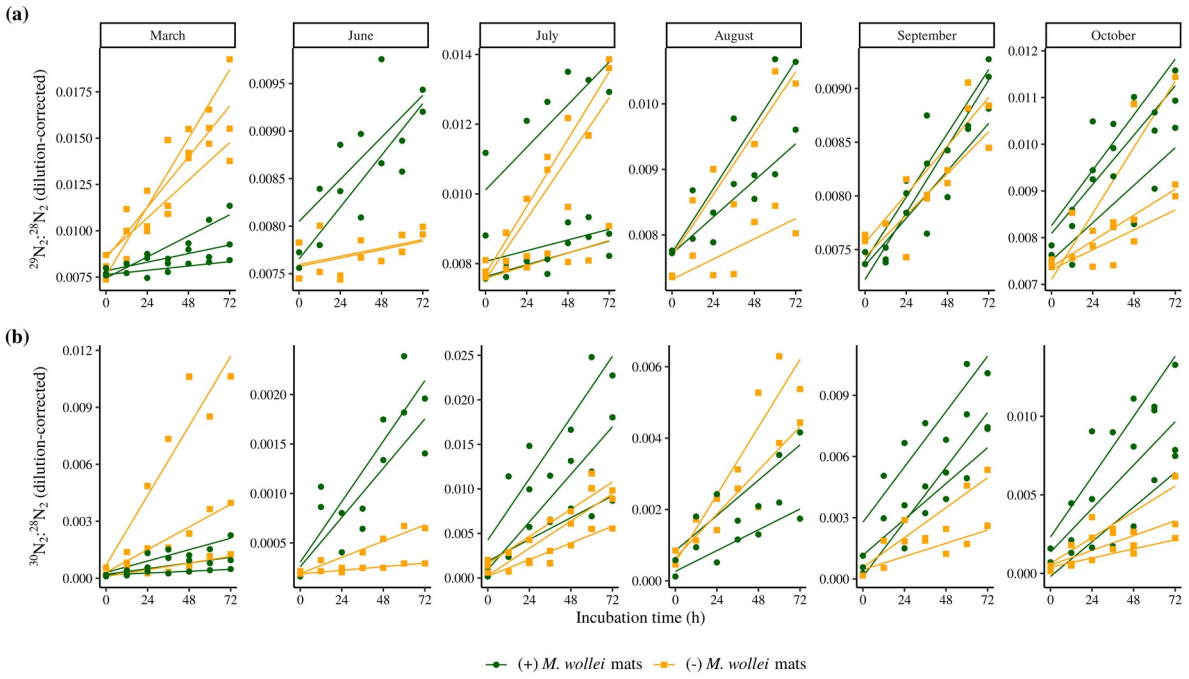


Figure S6. Time series of the dilution-corrected (a) $^{29}N_2$:$^{28}N_2$ and (b) $^{30}N_2$:$^{28}N_2$ ratios in the overlying water of the cores amended with $Na^{15}NO_3$, by month. Points are the individual samples of each core (green circles: cores with *M. wollei* mats; orange squares: cores without mats) and lines are the ordinary least-squares fits of each core, whose slopes give the potential denitrification rates (Eqs. (S1a)–(S5)). The $^{30}N_2$:$^{28}N_2$ ratio increased significantly ($p < 0.05$) in all 25 June–October cores and the $^{29}N_2$:$^{28}N_2$ ratio in 19 of them (r^2 = 0.67–0.97 and 0.58–0.97, respectively; 0.18–0.63 for the other six $^{29}N_2$:$^{28}N_2$ fits). The October cores without mats were not sampled at 60 h. March cores are shown for completeness.

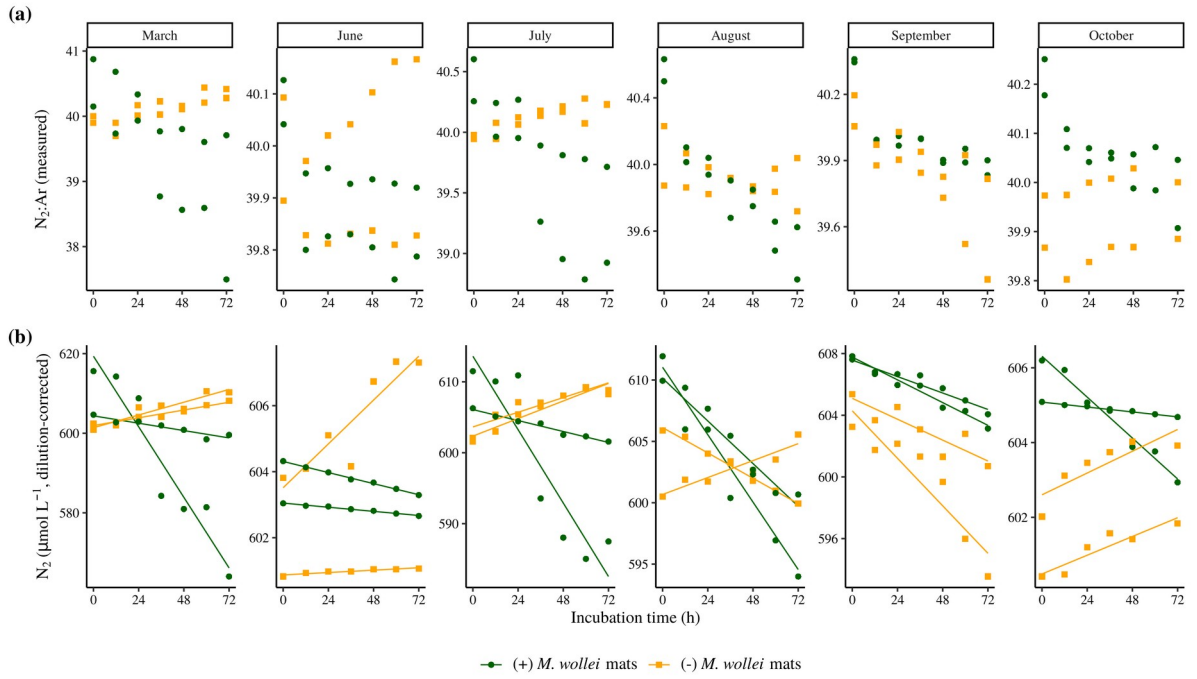


Figure S7. Time series of (a) the measured N_2:Ar ratio and (b) the dilution-corrected N_2 concentration (Eq. (S1b)) in the overlying water of the unamended control cores, by month (green circles: cores with *M. wollei* mats; orange squares: cores without mats). Lines in (b) are the ordinary least-squares fits of each core, whose slopes give the net N_2 fluxes (Eq. (S7)); the slope differed from zero ($p < 0.05$) in all 20 June–October cores ($r^2 = 0.72$–1.00). March cores are shown for completeness.

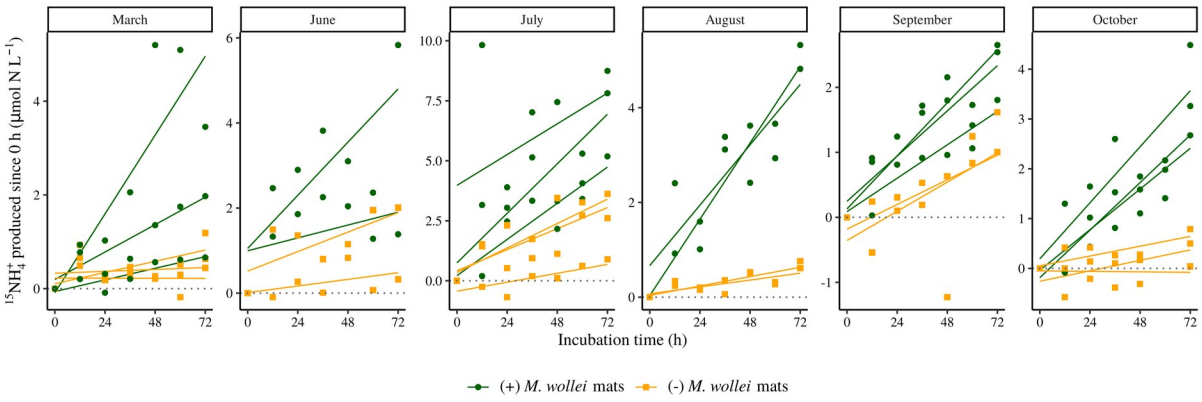


Figure S8. Time series of the $^{15}NH_4^+$ produced since the start of the incubation in the overlying water of the cores amended with $Na^{15}NO_3$ (from our $^{15}NH_4^+$ calibration following Yin et al., 2014, corrected at each sampling for the water replaced after the previous sampling; Sect. S1.3), by month (green circles: cores with *M. wollei* mats; orange squares: cores without mats). Lines are the ordinary least-squares fits of each core, whose slopes give the $^{15}NH_4^+$ production rates (Eq. (S6a)) from which the potential DNRA rates are derived (Eq. (S6b)); $^{15}NH_4^+$ increased significantly ($p < 0.05$) in 16 of the 25 June–October cores ($r^2 = 0.59$–0.94; 0.00–0.61 in the other nine). March cores are shown for completeness.

Supplementary tables

Table S1. Monthly means (± SD of replicate cores) of all core-based measurements. (a) Mat thickness and N-cycling rates (potential denitrification, potential DNRA scaled to the whole NO_3^- pool with the unscaled $^{15}NH_4^+$ production in parentheses (Sect. S1.3), and the net N_2 flux). Net N_2 fluxes are given in µmol N m^{-2} h^{-1} (converted from µmol N_2 m^{-2} h^{-1}); positive values indicate a net flux from the sediment to the water column and negative values a net flux from the water column into the sediment (net N_2 uptake). March data are shown for completeness but were excluded from the statistical analyses. Replicate cores per month and site type: denitrification and DNRA, n = 2 in June and August and in September without mats, n = 3 otherwise; net N_2 flux, n = 2.

Month	**Mats**	**Mat thickness (cm)**	**Denitrification (µmol N m^{-2} h^{-1})**	DNRA (µmol N m^{-2} h^{-1})	**Net N_2 flux (µmol N m^{-2} h^{-1})**
March	With	3.2 ± 0.8	7.4 ± 6.0	12.2 ± 12.8 (4.4 ± 4.2)	−129.3 ± 150.3
June	With	0.8 ± 0.4	4.6 ± 0.9	4.7 ± 3.0 (2.6 ± 2.2)	−2.4 ± 2.0
July	With	2.7 ± 0.3	34.5 ± 13.8	15.8 ± 1.8 (8.4 ± 0.8)	−59.8 ± 61.8
August	With	1.0 ± 0.2	10.5 ± 2.6	17.1 ± 0.3 (7.1 ± 0.3)	−40.5 ± 20.4
September	With	1.6 ± 0.5	27.9 ± 6.9	13.8 ± 2.1 (5.4 ± 0.9)	−9.5 ± 2.2
October	With	1.5 ± 0.3	32.3 ± 8.3	12.7 ± 2.0 (6.7 ± 1.5)	−7.4 ± 7.6
March	Without	–	59.1 ± 18.6	1.6 ± 2.1 (0.7 ± 0.9)	46.3 ± 19.3
June	Without	–	1.9 ± 1.0	4.8 ± 3.8 (2.4 ± 2.1)	9.0 ± 10.8
July	Without	–	30.9 ± 7.0	8.6 ± 1.7 (4.5 ± 1.2)	38.2 ± 10.1
August	Without	–	24.6 ± 11.4	4.6 ± 0.6 (1.6 ± 0.4)	−6.8 ± 39.0
September	Without	–	18.0 ± 9.1	9.1 ± 1.8 (4.2 ± 1.0)	−47.5 ± 27.2
October	Without	–	16.6 ± 10.9	2.4 ± 2.1 (1.0 ± 0.9)	11.0 ± 0.4

(b) Rates of change of nutrient concentrations in the overlying water during the ^{15}N incubations (linear slopes, mg L^{-1} h^{-1}; N for NH_4^+, NO_2^-, NO_3^- and P for PO_4^{3-}). Samples were not filtered before freezing (Sect. 2.3.1 of the main text), so these slopes are reported as supporting information.

Month	**Mats**	**NH_4^+**	**NO_2^-**	**NO_3^-**	**PO_4^{3-}**
March	With	0.0052 ± 0.0037	−0.0048 ± 0.0039	0.0004 ± 0.0001	0.0000 ± 0.0001
June	With	0.0025 ± 0.0004	−0.0045 ± 0.0026	−0.0001 ± 0.0000	−0.0001 ± 0.0001
July	With	0.0029 ± 0.0016	−0.0028 ± 0.0013	0.0001 ± 0.0002	0.0000 ± 0.0001
August	With	0.0035 ± 0.0007	−0.0029 ± 0.0017	0.0003 ± 0.0000	0.0000 ± 0.0000
September	With	0.0024 ± 0.0009	−0.0050 ± 0.0036	0.0000 ± 0.0001	−0.0001 ± 0.0000
October	With	0.0052 ± 0.0012	−0.0013 ± 0.0011	0.0000 ± 0.0001	0.0000 ± 0.0001
March	Without	0.0005 ± 0.0002	−0.0022 ± 0.0021	0.0000 ± 0.0000	0.0000 ± 0.0000
June	Without	0.0013 ± 0.0018	−0.0018 ± 0.0017	0.0000 ± 0.0001	−0.0001 ± 0.0000
July	Without	0.0020 ± 0.0014	−0.0034 ± 0.0021	0.0000 ± 0.0000	0.0022 ± 0.0041
August	Without	0.0025 ± 0.0007	−0.0062 ± 0.0021	0.0000 ± 0.0000	0.0044 ± 0.0063
September	Without	0.0024 ± 0.0005	−0.0014 ± 0.0005	0.0000 ± 0.0001	−0.0002 ± 0.0000
October	Without	0.0006 ± 0.0010	−0.0036 ± 0.0019	0.0000 ± 0.0001	0.0000 ± 0.0000

(c) Initial nutrient concentrations in the overlying water at the start of the incubations (mg N L^{-1}; mg P L^{-1} for PO_4^{3-}). The June mean of NH_4^+ with mats is driven by one of the two cores (1.291 and 0 mg N L^{-1}).

Month	Mats	NH_4^+	NO_2^-	NO_3^-	PO_4^{3-}
March	With	0.357 ± 0.192	0.053 ± 0.025	1.075 ± 0.322	0.015 ± 0.011
June	With	0.646 ± 0.913	0.008 ± 0.002	0.740 ± 0.409	0.014 ± 0.008
July	With	0.858 ± 0.249	0.002 ± 0.001	0.620 ± 0.082	0.011 ± 0.007
August	With	0.928 ± 0.077	0.008 ± 0.002	0.974 ± 0.049	0.014 ± 0.001
September	With	0.765 ± 0.530	0.016 ± 0.002	1.122 ± 0.494	0.030 ± 0.002
October	With	0.870 ± 0.384	0.013 ± 0.003	0.639 ± 0.153	0.017 ± 0.009
March	Without	0.011 ± 0.020	0.016 ± 0.000	0.960 ± 0.046	0.021 ± 0.009
June	Without	0.049 ± 0.069	0.012 ± 0.007	0.761 ± 0.173	0.012 ± 0.010
July	Without	0.542 ± 0.289	0.004 ± 0.002	0.669 ± 0.141	0.010 ± 0.003
August	Without	0.272 ± 0.069	0.013 ± 0.000	1.349 ± 0.237	0.020 ± 0.012
September	Without	0.000 ± 0.000	0.017 ± 0.001	0.837 ± 0.057	0.035 ± 0.003
October	Without	0.000 ± 0.000	0.015 ± 0.002	0.934 ± 0.028	0.011 ± 0.002

(d) Surface sediment (0–1 cm) characteristics.

Month	Mats	% N	% C	Porosity	Median grain size (mm)
March	With	0.21 ± 0.25	3.25 ± 3.17	0.74	0.063
June	With	0.33 ± 0.39	4.50 ± 2.88	0.74	0.063
July	With	0.11 ± 0.10	1.85 ± 0.99	0.87	0.063
August	With	0.08 ± 0.07	0.75 ± 0.52	0.87	0.063
September	With	0.08 ± 0.09	0.93 ± 0.93	0.74	0.063
October	With	0.75 ± 0.14	3.59 ± 0.99	0.87	0.063
March	Without	0.02 ± 0.02	0.18 ± 0.09	0.38	1
June	Without	0.02 ± 0.01	0.19 ± 0.03	0.38	1
July	Without	0.10 ± 0.10	1.46 ± 1.22	0.36	0.125
August	Without	0.11 ± 0.11	1.22 ± 1.07	0.36	0.125
September	Without	0.07 ± 0.00	0.73 ± 0.05	0.38	1
October	Without	0.17 ± 0.03	1.92 ± 0.49	0.36	0.125

Table S2. Dissolved O_2 in the overlying water of all incubated cores ($^{15}NO_3^-$-amended, $^{15}NH_4^+$-amended, and unamended control cores pooled), by month and mat presence: mean ± SD of the initial and final (72 h) concentrations, the lowest single reading, and the mean ± SD rate of change over the incubation (linear slope of O_2 vs. time for each core). Concentrations in µmol O_2 L^{-1} (1 mg L^{-1} = 31.25 µmol L^{-1}). In July the first reading was taken at 12 h; ten further readings are missing (August $^{15}NO_3^-$ core 2 without mats at 24 h, the June $^{15}NH_4^+$ core without mats at 36 h, October $^{15}NO_3^-$ core 1 and the October $^{15}NH_4^+$ core without mats at 0 h, and the six October cores without mats at 60 h); readings were not taken when the probe had not equilibrated, when the water level in the core was too low for the probe, or when the reading did not stabilize. In total, 377 readings were taken from June to October.

Month	Mats	*n* cores	Initial O_2	Final O_2	Minimum O_2	Rate of change (µmol L^{-1} h^{-1})
June	With	6	182 ± 95	141 ± 40	38	−0.60 ± 0.92
June	Without	6	188 ± 64	163 ± 58	78	−0.46 ± 0.53
July	With	6	106 ± 39	145 ± 31	40	+0.58 ± 0.19
July	Without	6	183 ± 37	179 ± 26	125	−0.16 ± 0.65
August	With	5	163 ± 34	141 ± 31	108	−0.32 ± 0.30
August	Without	5	236 ± 25	181 ± 25	157	−0.78 ± 0.48
September	With	6	202 ± 22	175 ± 25	141	−0.43 ± 0.09
September	Without	5	249 ± 24	200 ± 17	186	−0.68 ± 0.27
October	With	6	184 ± 37	111 ± 17	85	−0.99 ± 0.65
October	Without	6	230 ± 23	197 ± 37	134	−0.47 ± 0.36
June–October	With	29	167 ± 60	143 ± 35	38	−0.35 ± 0.73
June–October	Without	28	215 ± 45	184 ± 36	78	−0.49 ± 0.50
March	With	5	159 ± 18	75 ± 24	42	−0.97 ± 0.57
March	Without	5	246 ± 11	181 ± 26	133	−1.00 ± 0.15

Table S3. Two-way ANOVA (Type III sums of squares) for depth-integrated porewater nutrient concentrations (mg L^{-1} cm; Sect. 2.4) in the mat horizon, fitted separately for each month with mat presence, light condition and their interaction as fixed factors. p_{adj} are Holm-adjusted *p*-values for the family of five monthly tests per nutrient and factor; adjusted $p \le 0.05$ in bold. Degrees of freedom are 1 and 4 for every *F* test.

Nutrient	Month	R^2	Mat $F_{1,4}$	*p*	p_{adj}	Light $F_{1,4}$	*p*	p_{adj}	Mat × light $F_{1,4}$	*p*	p_{adj}
NH_4^+	June	0.96	51.10	0.002	**0.010**	0.60	0.483	1.000	0.53	0.508	1.000
	July	0.75	4.28	0.107	0.429	0.00	1.000	1.000	6.02	0.070	0.351
	August	0.44	0.74	0.437	0.875	0.40	0.563	1.000	0.20	0.679	1.000
	September	0.90	3.33	0.142	0.429	4.70	0.096	0.480	1.52	0.285	1.000
	October	0.25	0.66	0.463	0.875	0.00	1.000	1.000	0.00	1.000	1.000
NO_2^-	June	0.64	4.23	0.109	0.327	0.15	0.722	1.000	0.07	0.800	1.000
	July	0.04	0.09	0.782	0.782	0.00	1.000	1.000	0.00	1.000	1.000
	August	0.87	2.97	0.160	0.327	26.67	0.007	**0.033**	9.95	0.034	0.172
	September	0.85	12.80	0.023	0.116	0.01	0.941	1.000	8.97	0.040	0.172
	October	0.85	10.80	0.030	0.121	17.74	0.014	0.054	6.87	0.059	0.176

Nutrient	Month	R^2	Mat $F_{1,4}$	p	p_{adj}	Light $F_{1,4}$	p	p_{adj}	Mat × light $F_{1,4}$	p	p_{adj}
NO_3^-	June	0.94	30.63	0.005	**0.021**	0.00	1.000	1.000	0.08	0.787	1.000
	July	0.96	48.80	0.002	**0.011**	0.76	0.432	1.000	0.23	0.657	1.000
	August	0.25	0.58	0.490	0.869	0.06	0.814	1.000	0.00	0.980	1.000
	September	0.56	1.49	0.290	0.869	0.69	0.452	1.000	0.13	0.738	1.000
	October	0.90	1.17	0.340	0.869	0.05	0.828	1.000	16.71	0.015	0.075
PO_4^{3-}	June	1.00	22785	< 0.001	**< 0.001**	10.78	0.030	0.152	7.43	0.053	0.263
	July	0.98	80.87	< 0.001	**0.003**	0.87	0.404	1.000	0.43	0.546	0.795
	August	0.33	0.95	0.385	0.770	1.79	0.252	1.000	0.90	0.397	0.795
	September	0.85	5.12	0.086	0.259	0.95	0.385	1.000	1.78	0.253	0.758
	October	0.64	0.22	0.663	0.770	0.70	0.451	1.000	4.36	0.105	0.421
Total Fe	June	0.91	20.85	0.010	**0.031**	0.00	1.000	1.000	0.00	1.000	1.000
	July	0.53	4.26	0.108	0.216	0.88	0.401	1.000	2.69	0.177	0.883
	August	0.15	0.49	0.522	0.522	0.00	1.000	1.000	0.03	0.861	1.000
	September	0.99	322.17	< 0.001	**< 0.001**	0.00	1.000	1.000	0.00	0.975	1.000
	October	0.99	181.46	< 0.001	**< 0.001**	1.00	0.374	1.000	0.47	0.532	1.000

Concentrations were integrated by trapezoidal integration over the 0–2 cm interval below the sediment–water interface (0–1 cm in August), chosen to encompass the mat horizon of the porewater cores; the same interval was used in cores without mats. Nutrients are listed in the order NH_4^+, NO_2^-, NO_3^-, PO_4^{3-}, Fe throughout the Supplement.

Table S4. Primary test of the mat effect: paired (one-sample) *t* procedures on the monthly mean differences (with mats minus without mats) across the five growing-season sampling events (June–October 2023; df = 4). Rates in μmol N m^{-2} h^{-1}; nutrient concentrations in mg N L^{-1}. Net N_2 flux values have been converted from μmol N_2 to μmol N.

Variable	Mean difference	t_4	p	95 % CI lower	95 % CI upper
Initial NH_4^+	0.64	6.85	0.002	0.38	0.90
Initial NO_2^-	−0.0028	−3.36	0.028	−0.0051	−0.0005
Initial NO_3^-	−0.09	−0.78	0.478	−0.41	0.23
Denitrification	3.5	0.71	0.517	−10.3	17.4
DNRA	6.9	3.17	0.034	0.9	13.0
Net N_2 flux	−24.7	−1.13	0.323	−85.5	36.1

Each response variable was treated as a separate a priori hypothesis; no adjustment for multiple comparisons was applied across variables.

Table S5. Exploratory month-specific comparisons of initial overlying-water nutrient concentrations (mg N L^{-1}) and N-cycling rates (potential denitrification, potential DNRA, and net N_2 flux; μmol N m^{-2} h^{-1}) between cores with and without *M. wollei* mats (unequal-variance two-sample *t*-tests). p_{adj} are Holm-adjusted *p*-values for the family of five monthly tests per variable. Net N_2 flux confidence limits have been converted from μmol N_2 m^{-2} h^{-1} to μmol N m^{-2} h^{-1}. The July, August, and October DNRA differences have an adjusted $p \le 0.05$. With two or three cores per group (df ≈ 1–4), these tests have little power and are shown for completeness.

Variable	Month	t	df	p	p_{adj}	95 % CI lower	95 % CI upper
Initial NH_4^+	June	0.92	1.01	0.524	0.524	−7.41	8.61

Variable	Month	*t*	df	*p*	p_{adj}	95 % CI lower	95 % CI upper
	July	1.44	3.92	0.226	0.451	−0.30	0.93
	August	8.94	1.98	0.013	0.064	0.34	0.97
	September	2.50	2.00	0.130	0.389	−0.55	2.08
	October	3.92	2.00	0.059	0.237	−0.08	1.82
Initial NO_2^-	June	−0.80	1.15	0.556	1.000	−0.05	0.04
	July	−1.78	2.82	0.179	0.857	−0.01	0.00
	August	−3.49	1.03	0.171	0.857	−0.02	0.01
	September	−0.60	2.71	0.592	1.000	−0.01	0.00
	October	−0.93	3.71	0.408	1.000	−0.01	0.00
Initial NO_3^-	June	−0.07	1.34	0.954	1.000	−2.25	2.21
	July	−0.52	3.21	0.636	1.000	−0.34	0.24
	August	−2.19	1.08	0.257	1.000	−2.19	1.44
	September	0.99	2.08	0.422	1.000	−0.91	1.48
	October	−3.29	2.13	0.075	0.373	−0.66	0.07
Denitrification	June	2.89	1.96	0.104	0.519	−1.40	6.83
	July	0.40	2.97	0.717	0.964	−25.11	32.26
	August	−1.70	1.10	0.321	0.964	−98.78	70.61
	September	1.30	1.79	0.335	0.964	−26.64	46.36
	October	1.98	3.74	0.124	0.519	−6.90	38.21
DNRA	June	−0.01	1.88	0.994	0.994	−15.72	15.67
	July	5.03	3.97	0.007	0.026	3.22	11.20
	August	25.20	1.47	0.006	0.026	9.38	15.45
	September	2.67	2.55	0.090	0.179	−1.49	10.86
	October	6.24	4.00	0.003	0.017	5.76	14.98
Net N_2 flux	June	−1.46	1.07	0.371	1.000	−96.57	73.88
	July	−2.21	1.05	0.260	1.000	−597.18	401.15
	August	−1.08	1.51	0.422	1.000	−219.17	151.87
	September	1.97	1.01	0.297	1.000	−200.20	276.10
	October	−3.39	1.01	0.181	0.906	−86.10	49.39

Table S6. Correlations between the N-cycling rates (potential denitrification, potential DNRA, and net N_2 flux) and the initial concentrations of NH_4^+, NO_2^- and NO_3^- in the overlying water at the start of the incubations (June–October cores). Initial concentrations are those of the individual cores (n = 25 cores for denitrification and DNRA); the unamended control cores (n = 20) were matched to the ^{15}N-amended core with the same number from the same month and site type. The correlations are exploratory and were not adjusted for multiple comparisons; with a Holm adjustment over the three nutrients of each rate, only the DNRA–NH_4^+ correlation remains significant (adjusted p = 0.002 and 0.003 for the Spearman and the Pearson coefficient).

Rate	Initial concentration	Spearman ρ	*p*	Pearson *r*	*p*
Denitrification	NH_4^+	0.19	0.376	0.17	0.411
	NO_2^-	−0.14	0.505	−0.13	0.531
	NO_3^-	−0.22	0.300	−0.15	0.477
DNRA	NH_4^+	0.63	< 0.001	0.62	0.001
	NO_2^-	−0.21	0.314	−0.25	0.234
	NO_3^-	−0.25	0.224	−0.18	0.401
Net N_2 flux	NH_4^+	−0.18	0.460	−0.16	0.504
	NO_2^-	−0.04	0.866	0.06	0.811
	NO_3^-	0.03	0.916	0.05	0.839

References

Dong, L. F., Smith, C. J., Papaspyrou, S., Stott, A., Osborn, A. M., and Nedwell, D. B.: Changes in benthic denitrification, nitrate ammonification, and anammox process rates and nitrate and nitrite reductase gene abundances along an estuarine nutrient gradient (the Colne estuary, United Kingdom), Appl. Environ. Microbiol., 75, 3171–3179, https://doi.org/10.1128/AEM.02511-08, 2009.

Gardner, W. S., McCarthy, M. J., An, S., Sobolev, D., Sell, K. S., and Brock, D.: Nitrogen fixation and dissimilatory nitrate reduction to ammonium (DNRA) support nitrogen dynamics in Texas estuaries, Limnol. Oceanogr., 51, 558–568, https://doi.org/10.4319/lo.2006.51.1_part_2.0558, 2006.

Hamme, R. C. and Emerson, S. R.: The solubility of neon, nitrogen and argon in distilled water and seawater, Deep-Sea Res. Pt. I, 51, 1517–1528, https://doi.org/10.1016/j.dsr.2004.06.009, 2004.

Kana, T. M., Darkangelo, C., Hunt, M. D., Oldham, J. B., Bennett, G. E., and Cornwell, J. C.: Membrane inlet mass spectrometer for rapid high-precision determination of N_2, O_2, and Ar in environmental water samples, Anal. Chem., 66, 4166–4170, https://doi.org/10.1021/ac00095a009, 1994.

McCarthy, M. J., Gardner, W. S., Lehmann, M. F., Guindon, A., and Bird, D. F.: Benthic nitrogen regeneration, fixation, and denitrification in a temperate, eutrophic lake: effects on

the nitrogen budget and cyanobacteria blooms, Limnol. Oceanogr., 61, 1406–1423, https://doi.org/10.1002/lno.10306, 2016.

Nielsen, L. P.: Denitrification in sediment determined from nitrogen isotope pairing, FEMS Microbiol. Ecol., 86, 357–362, https://doi.org/10.1111/j.1574-6968.1992.tb04828.x, 1992.

Risgaard-Petersen, N. and Rysgaard, S.: Nitrate reduction in sediments and waterlogged soil measured by ^{15}N techniques, in: Methods in Applied Soil Microbiology and Biochemistry, edited by: Alef, K. and Nannipieri, P., Academic Press, London, 287–295, 1995.

Risgaard-Petersen, N., Nielsen, L. P., Rysgaard, S., Dalsgaard, T., and Meyer, R. L.: Application of the isotope pairing technique in sediments where anammox and denitrification coexist, Limnol. Oceanogr.-Meth., 1, 63–73, https://doi.org/10.4319/lom.2003.1.63, 2003.

Song, G. D., Liu, S. M., Kuypers, M. M. M., and Lavik, G.: Application of the isotope pairing technique in sediments where anammox, denitrification, and dissimilatory nitrate reduction to ammonium coexist, Limnol. Oceanogr.-Meth., 14, 801–815, https://doi.org/10.1002/lom3.10127, 2016.

Yin, G., Hou, L., Liu, M., Liu, Z., and Gardner, W. S.: A novel membrane inlet mass spectrometer method to measure $^{15}NH_4^+$ for isotope-enrichment experiments in aquatic ecosystems, Environ. Sci. Technol., 48, 9555–9562, https://doi.org/10.1021/es501261s, 2014.